Wide solid-discharge fluctuations and collective effects in bed-load transport

C. Ancey
École Polytechnique Fédérale de Lausanne, Ecublens, 1015 Lausanne, Switzerland
T. Böhm & P. Frey
Cemagref, Domaine Universitaire BP 76, 38402 Saint-Martin-d'Hères Cedex, France
M. Jodeau
Cemagref, 3 bis quai Chauveau, 69336 Lyon, France

Observations in rivers or flumes have shown that for low water discharge, sediment transport is a very intermittent process. To understand the physical origins of the solid-discharge fluctuations, we investigated the motion of coarse spherical glass beads entrained by a steady shallow turbulent water flow down a steep two-dimensional channel with a mobile bed and steady bead supply at the inlet. Flows were filmed from the side by a high-speed camera. We also revisited Einstein's theory on sediment and derived the statistical properties of the key flow variables. Analyzing the autocorrelation functions and the probability distributions of our measurements revealed the existence of long-range correlations. These frequent wide fluctuations stemmed particle entrainment and motion being collective phenomena rather than individual processes, contrary to what is assumed in most theoretical models.

1 INTRODUCTION

The objective of this paper is to characterize and understand the physical origins of wide fluctuations in the solid discharge for sediment transport in gravel-bed rivers and mountain torrents. Sediment is assumed to be made up of coarse particles driven by gravity and drag exerted by a water turbulent flow.

Despite substantial progress made over the last two decades in the physical understanding of the motion of coarse particles in a turbulent stream, the ability to compute sediment flux in rivers remains poor. For instance, the sediment flow rates measured in gravel-bed rivers differ within one to two orders of magnitude from the bed-load transport equations (Wilcock 2001; Martin 2003; Barry et al. 2004), even though these equations have been established from flume experiments using regression techniques and are believed to provide a proper evaluation of sediment transport in a well-controlled laboratory environment.

Impediments to a full analytical approach to two-phase flows are many: complex interplay between the particles and the carrying fluid, particle exchanges between the bed and the flow, turbulence effects (bed friction, advection of turbulent structures), etc. That is why most models are based on substantial approximations of the interplay between the solid and fluid phases.

Einstein (1950) realized how important it is to account for the episodic nature of particle transport in computing the solid discharge. In Einstein's view, sediment transport does not result from an equilibrium in the momentum transfers between solid and liquid phases (Bagnold's assumption), but rather from the difference between the entrainment and deposition rates. Einstein's stochastic approach raises a number of issues that have received few responses to date. For instance, since particles move sporadically and in different groups, the solid flow rate is made up of a series of pulses and is highly fluctuating, which makes it difficult to define and measure it properly, even under steady flow conditions (Bunte & Abt 2005). Both field and laboratory experiments have revealed that instances in which the instantaneous solid discharge is four times higher than its mean value are frequent (Kuhnle & Southard 1988; Lisle 1989; Boehm et al. 2004). Translated statistically, this observation means that the probability density functions of the transport-rate records have a thick tail and depart from the expected Gaussian behavior. This departure can be seen as the hallmark of collective motions (Sornette 2000); if so, this also implies that any mean-field approximation runs into difficulty since cooperation between particles is not accounted for.

Our idea was to run experiments in an inclined,

two-dimensional flume with a continuous particle supply and steady flow rate. This two-dimensional flume is assumed to be the simplest representation of sediment transport on the laboratory scale and presents overwhelming advantages: the boundary conditions can be controlled and most of the flow variables can be measured using image processing. Since a quantitative comparison between theory and experiment is biased by any parameter fitting, we tested Einstein's theory by analyzing the probability distributions and correlations of the signals measured.

2 EINSTEIN'S THEORY REVISITED

Using *ad hoc* arguments, Einstein (1950) derived a bed-load equation, which has been considered as the cornerstone of probabilistic theories of bed-load transport. Taking inspiration from the work done by Lisle et al. (1998) and Papanicolaou et al. (2002), we assume that sediment transport at low flow rates can be described using a birth-death process.

The solid discharge can be defined as the flux of particles through a flow cross-section $\mathcal{S}$. Equivalently, we can define the flow rate $\dot{n} = q_s/v_p$ as the number n of particles in motion within a control volume of length L times their respective velocity u_i

$$\dot{n} = \frac{1}{L}\sum_{i=1}^{n} u_i, \tag{1}$$

(Boehm et al. 2004). In order to compute the discharge equation, we need to establish (i) the number n of particles in motion and (ii) their velocities depending on the control parameters (water discharge q_w, θ, particle radius a, particle density ρ_p).

In order to compute the number of particles in motion, we can draw an analogy with chemical reactions. If the particles resting on the bed surface are denoted by B, the moving particles by M, we can represent the exchanges between the two phases in the following way: $B \rightleftarrows M$. From these equations, we can establish a kinetic equation, which tells us the rate at which exchanges occur between the species B and M. The time variation in the number of moving particles is

$$\frac{dn}{dt} = \frac{n_{b\to m}}{t_b} - \frac{n_{m\to b}}{t_m}, \tag{2}$$

where $n_{b\to m}$ is the number of particles dislodged from the bed and $n_{m\to b}$ is the number of moving particles that are left to rest within the observation window. These population exchanges are associated with the characteristic times t_b and t_m, which are in turn related to the mean times during which a single particle stays at rest or moves, respectively σ and τ [see Fig. 1(a)]. We can also use Eq. (2) to define the entrainment rate (first term on the right-hand side) and the deposition rate (second on the right-hand side).

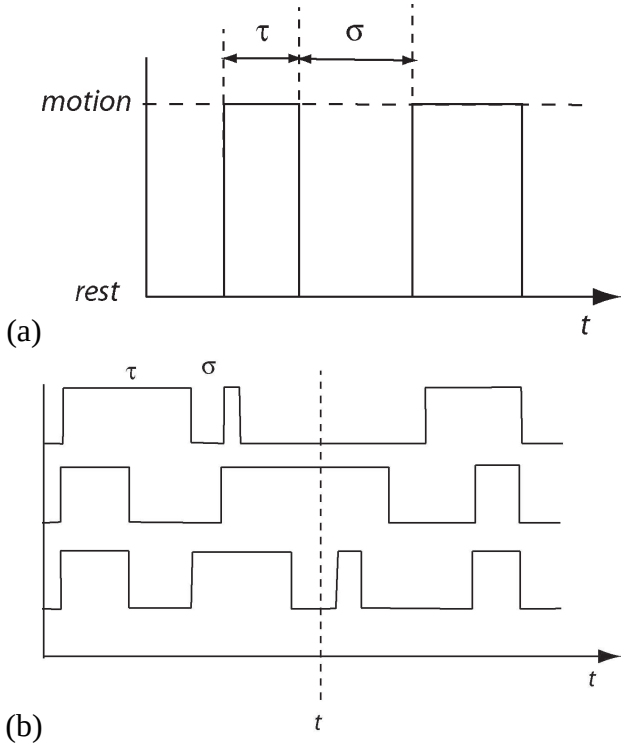

Figure 1. (a) Succession of resting and moving phases for a single particle. (b) The solid discharge is related to the sum of the state variables.

Transitions between the moving/resting states occur randomly. Following Lisle et al. (1998) and Papanicolaou et al. (2002), we assume that the particle motion is influenced only by its present state and has a fade memory of its previous states. In other words, the state transitions are governed by a continuous-time Markov process of order 1, with two discrete states (moving/resting). If we further assume that there is time and space invariance in the erosion/deposition process, the Markov transitions occur with constant probability per unit time. For any small time increment δt, we have

$$\text{Prob(moving at time } t+\delta t) = \sigma^{-1}\delta t + o(\delta t),$$

$$\text{Prob(resting at time } t+\delta t) = \tau^{-1}\delta t + o(\delta t),$$

where the characteristic times σ and τ are constant. This two-state Markov process is known as a telegrapher's process (Gardiner 1983). With these assumptions, it can be shown that the resting and moving times are exponentially distributed with means σ and τ, respectively. If $T_{b,i}$ and $T_{m,i}$ represent the durations of the *i*th periods of rest and motion since observation has started, then $\text{Prob}(T_m) = \tau^{-1}\exp(T_m/\tau)$ and $\text{Prob}(T_b) = \sigma^{-1}\exp(T_b/\sigma)$; said differently, the waiting time $\Delta t_{b\to r}$ between two entrainments is exponentially distributed with a mean time equal to σ: $\text{Prob}(\Delta t_{b\to r}) = (\sigma+\tau)^{-1}\exp(\Delta t_{b\to r}/(\sigma+\tau))$. Using the correspondence between the Poisson and exponential distributions, we also deduce that the number of events (deposition/entrainment) that occur per unit

time is distributed according to a Poisson distribution: the probability that we observe k entrainments of the same particle within the time interval δt (of any duration) is given by $\text{Prob}(k;\ \delta t) = \nu^k \exp^{-\nu}/k!$, with $\nu = \delta t/\sigma$. The autocorrelation function is $\rho(s) = \exp(-(1/\tau + 1/\sigma)s)$ (Gardiner 1983).

This description is a simplified probabilistic Lagrangian description of a single particle's motion. We generalize it to obtain a Eulerian viewpoint, where we describe the motion of n particles within an observation window. Within our observation window of length $L = 2\lambda a \gg a$ (λ being a free parameter that can take any value), we assume that on average, the particle flux is steady, which means that the particles that leave the window are replaced by other particles coming from upstream. Within this window, there are approximately $N = \lambda$ particles lying over the bed surface, either at rest or in motion. The number n of particles in motion is then the sum of N variables independently distributed and governed by a telegraph process [see Fig. 1(b)]. Since each particle is governed by a telegraph process, the probability of observing it in motion is $\xi = \tau/(\tau + \sigma)$, i.e., it follows a Bernoulli distribution. Now, summing N particles following a Bernoulli distribution leads to a binomial distribution with mean ξN and variance $\xi(1-\xi)N$. We then conclude that with our assumptions, the number n of moving particles is distributed according to a binomial distribution, which means that if ξ stays constant independently of the number of particles N when $L \to \infty$, then the probability distribution of n tends toward a Gaussian distribution. If we further assume that whenever a particle is set in motion, it reaches a fairly constant velocity u_p (Ancey et al. 2003), then using Eq. (1) leads to concluding that the probability distribution of the solid discharge is the binomial distribution Bi, with mean $\xi N u_p$ and variance $\xi(1-\xi)Nu_p^2$

$$\text{Prob}(\dot{n}) = \text{Bi}[\xi N u_p, \xi(1-\xi)Nu_p^2].$$

In the large N limit, this distribution tends to be Gaussian. Since the sum of Poisson-distributed variables also has a Poisson distribution, we infer that the number of deposition/entrainment events per unit time has a Poisson distribution: the probability that we observe k entrainments within the time interval δt is given by

$$\text{Prob}(k;\ \delta t) = \frac{\nu^k}{k!}\exp^{-\nu}, \tag{3}$$

with $\nu = N\delta t/\sigma$. Instead of the Poisson distribution for characterizing the number of events per unit time, we can equivalently use the exponential distribution for specifying the lag times between two events; the mean waiting times between two entrainments within the observation window is $(\sigma + \tau)/N$. The autocorrelation function of N parallel telegrapher's processes is

$$\rho(s) = \exp(-s/\tau_*), \tag{4}$$

with $\tau_* = \sigma\tau/(\tau + \sigma)/N$. It is worth noting that, with our assumptions, the solid discharge and the number of moving particles have the same autocorrelation function.

According to Einstein (1950), the probability of entrainment is the fraction of time $\xi = \tau/(\tau + \sigma)$ that a particle is in a moving state. It also represents, on average, the relative number of particles (i.e., p) that have moved within the observation window for a given time interval (Papanicolaou et al. 2002). Moreover, in Einstein-like theories, particle entrainment results from a loss of stability: when the instantaneous lift and/or drag force exceeds the resisting forces, the particle is dislodged from the bed and starts to roll. By relating the fluid forces to the instantaneous fluid velocity u_f, we can deduce the fluid threshold u_c corresponding to incipient motion (Papanicolaou et al. 2002; Marsh et al. 2004). The probability p is then defined as $p = \xi = \text{Prob}(u_f > u_c)$. Over the time interval t_b, the number of particles that are entrained is then $n_{b\to m} = Np$, while the number of particles that come to a halt is $n_{m\to b} = n(1-p)$ over the period t_m. In steady flow conditions, Eqs. (2) and (1) lead to

$$q_s = \frac{p}{1-p}\frac{t_m}{t_b}\frac{N}{L}u_p = \frac{p}{1-p}\frac{t_m}{t_b}\frac{u_p}{2a}, \tag{5}$$

which is formally similar to the solid-discharge equation derived by Einstein (1950), except that the solid discharge is now explicitly dependent on the particle velocity.

3 EXPERIMENTAL FACILITIES

3.1 *Overview*

In order to test the influence of fluid velocity (or, equivalently, Shields number) on bed-load transport, we ran six experiments with different flow rates in a two-dimensional channel (see Sect. 3.2). The features of each run are summarized in Table 1. The hydraulic conditions are specified using classic dimensionless numbers. The flow Reynolds number is defined as $Re = 4R_h\bar{u}_f/\nu$, where $R_h = Wh/(2h+W)$ denotes hydraulic radius, $\bar{u}_f = q_w/(Wh)$ mean fluid velocity, ν kinematic viscosity of water, and h the time-averaged water depth. The Froude number $Fr = \bar{u}_f/\sqrt{gh}$ varied significantly over the duration of the experiment and along the main stream direction. The mean Fr values are reported in Table 1. The Shields number is defined as $Sh = \rho_f\bar{u}_f^2/((\rho_p - \rho_f)gh)$ and reflects the ratio of the water driving force to the friction resistance force on the bed (Boehm et al. 2004). The solid concentration is defined as the ratio of the

solid and water discharges $C_s = q_s/q_w$. Values reported in Table 1 are low, which indicates that particle flow was dilute. The h/d ratio is low, typically in the range 1.7–3.2.

3.2 *Channel*

Experiments were carried out in a tilted, narrow, glass-sided channel, 2 m in length and 20 cm in height. Figure 2 shows a sketch of the experimental facility. The channel width W was adjusted to 6.5 mm, which was slightly larger than the particle diameter (6 mm). In this way, particle motion was approximately two-dimensional and stayed in the focal plane of the camera. The channel slope $\tan\theta$ was 10%.

3.3 *Channel base and mobile bed*

The channel base consisted of half-cylinders of equal size ($a = 3$ mm), but they were randomly arranged. Disorder was essential, as it prevented slipping of entire layers of particles on the upper bed surface.

3.4 *Solid and water supplies*

Colored spherical glass beads with a nominal diameter $2a$ of 6 mm and a density ρ_p of 2500 kg/m^3 were used. They were injected from a reservoir into the channel using a wheel driven by a direct current motor and equipped with 20 hollows on the circumference, as depicted in Fig. 2. For the experiments presented here, the injection rate $\dot{n}_0$ ranged from 5 to 20 beads per second, with an uncertainty of less than 5%. This corresponded to a solid discharge per unit width q_s/W of $9 - 38 \times 10^{-5}$ m^2/s. The water supply at the channel entrance was controlled by an electromagnetic flow meter. The discharge per unit width q_w/W ranged from 4 to 10×10^{-3} m^2/s. The hydraulic conditions (velocity profile, bed friction, etc.) have been specified in earlier papers (Ancey et al. 2002; Boehm et al. 2004).

3.5 *Experimental procedures*

Once bed equilibrium was reached, the particles and the water stream were filmed using a Pulnix partial scan video camera (progressive scan TM-6705AN). The camera was placed perpendicular to the glass panes at 115 cm away from the channel, approximately 80 cm upstream from the channel outlet. It was inclined at the same angle as the channel. Lights were positioned in the backside of the channel. An area of $L = 22.5$ cm in length and 8 cm in height was filmed and later reduced to accelerate image processing.

The camera resolution was 640×192 pixels for a frame rate of $f = 129.2$ fps (exposure time: 0.2 ms, 256 gray levels). Each sequence was limited to 8000 images due to limited computer memory; this corresponded to an observation duration of approximately 1 minute.

Each experiment was repeated at least twice in order to spot possible experimental problems and to get an idea of the data scattering. Images were analyzed using the WIMA software, provided by the *Traitement du Signal et Instrumentation* laboratory in Saint-Etienne (France). For more details, the reader can refer to (Boehm 2005).

4 EXPERIMENTAL RESULTS

As we shall see below (Sect. 4.1), the generalized Einstein theory predicts a number of features such as the nearly Gaussian distribution of the solid discharge, the Poissonian character of the occurrence of entrainment/deposition over time, and the exponential decrease in the autocorrelation function of the number of particles moving within the observation window. There are also a number of features that conflict with the fundamental assumptions underpinning this theory. In Sect. 4.2, we will see that the probability distributions of the key variables have much thicker tails than expected. This will be interpreted as the hallmark of cooperation processes between particles when they are entrained or when they move.

4.1 *Solid-discharge time series*

Figure 3 shows the time variations in the solid discharge $\dot{n}$, the number of particles n_r in a rolling regime, the number of particles that passed from a resting state to a rolling state ($r \to b$) and conversely ($b \to r$). This diagram represents the results obtained for a mean bed slope of 0.1 and a solid discharge at the flume inlet $\dot{n}_0 = 8$ beads/s (experiment 10-8 in Table 1); these plots are typical of the results that we obtained for other solid discharges $\dot{n}_0$.

Note that in these state transitions [see Fig. 3(d–e)], more than one particle can be involved; because of the limitation of the acquisition rate of our high-speed camera (130 images per second), we could not resolve two events that occurred over very short time intervals. This limitation may pose problems when interpreting the Markovian properties of our time series.

A striking point in Fig. 3 is the wide fluctuations that all the time series exhibit. Typically, the solid flow rate ranged from 0 to 22 beads/s, while the mean flow rate imposed at the inlet was $\dot{n}_0 = 8$ beads/s. For the rolling regime, the fluctuation range was 0–40 beads within the observation window, whereas the mean number was $\bar{n}_r = 9.7$ beads.

As shown in Fig. 4(a), the empirical probability distribution of solid discharge is closely approximated by a Gaussian distribution, although, in places, there are spikes departing from the Gaussian trend. These spikes reflect the existence of a finite number of particles within the observation window (Boehm et al. 2004). This Gaussian behavior is expected since the solid discharge is defined as the product of the num-

Experiment	E10-6	E10-7	E10-8	E10-9	E10-16	E10-21
$\tan\theta$ (%)	10.0	10.0	10.0	10.0	10.0	10.0
$\dot{n}_0$ (beads/s)	5.3	6.7	8.0	10.0	15.4	20.0
q_w/W (10^{-3} m^2/s)	4.15	4.42	5.38	5.54	8.19	10.31
h (mm)	10.2	10.6	12.2	12.3	16.6	19.1
$\bar{u}_f$ (m/s)	0.41	0.42	0.44	0.45	0.49	0.54
$\dot{n}$ (beads/s)	5.72	6.85	7.74	9.41	15.56	20.57
Re	4020	4090	4550	4570	5280	5910
Fr	1.29	1.29	1.28	1.30	1.22	1.25
Sh	0.113	0.120	0.135	0.139	0.188	0.216
C_s (%)	2.40	2.69	2.50	2.96	3.30	3.47
$\bar{u}_r$ (m/s)	0.063	0.074	0.065	0.075	0.075	0.072
$\bar{u}_s$ (m/s)	0.28	0.29	0.29	0.29	0.32	0.32
n_r	7.29	6.92	10.37	9.94	16.65	26.69
Var(n_r)	59.13	32.72	55.82	42.61	69.37	119.06
n_s	2.17	2.93	3.39	3.74	6.19	7.52
Var(n_s)	2.40	2.87	3.14	3.30	4.88	5.44
t_e (s)	0.34	0.36	0.23	0.22	0.20	0.18

Table 1. Flow characteristics and time-averaged values of dimensionless numbers characterizing bed load and water flow. The slope is kept constant: $\tan\theta = 10\%$, while the solid discharge at the inlet $\dot{n}_0$ is altered. The notation E10-6 means: $\tan\theta = 10\%$ and $\dot{n}_0 \approx 6$ beads/s. The measured solid discharge within the observation window is denoted by $\dot{n}$. Re, Fr, and Sh are the Reynolds, Froude, and Shields dimensionless numbers. The time-averaged particle velocity in the rolling (saltating, respectively) regime is denoted by $\bar{u}_r$ ($\bar{u}_s$, respectively), while n_r (n_s, respectively) represents the mean number of rolling (saltating, respectively) particles; the variance (Var) of n_r and n_s is provided. We have also reported the autocorrelation time t_e of the rolling-particle number $n_r(t)$.

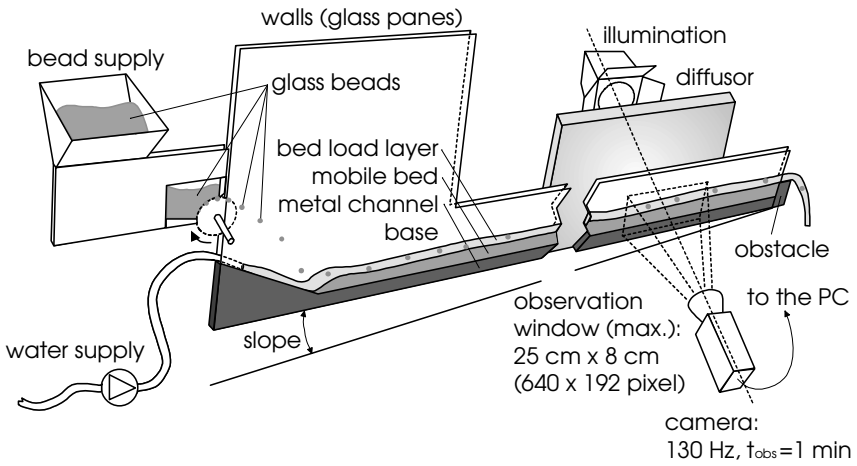

Figure 2. Sketch of the experimental setup.

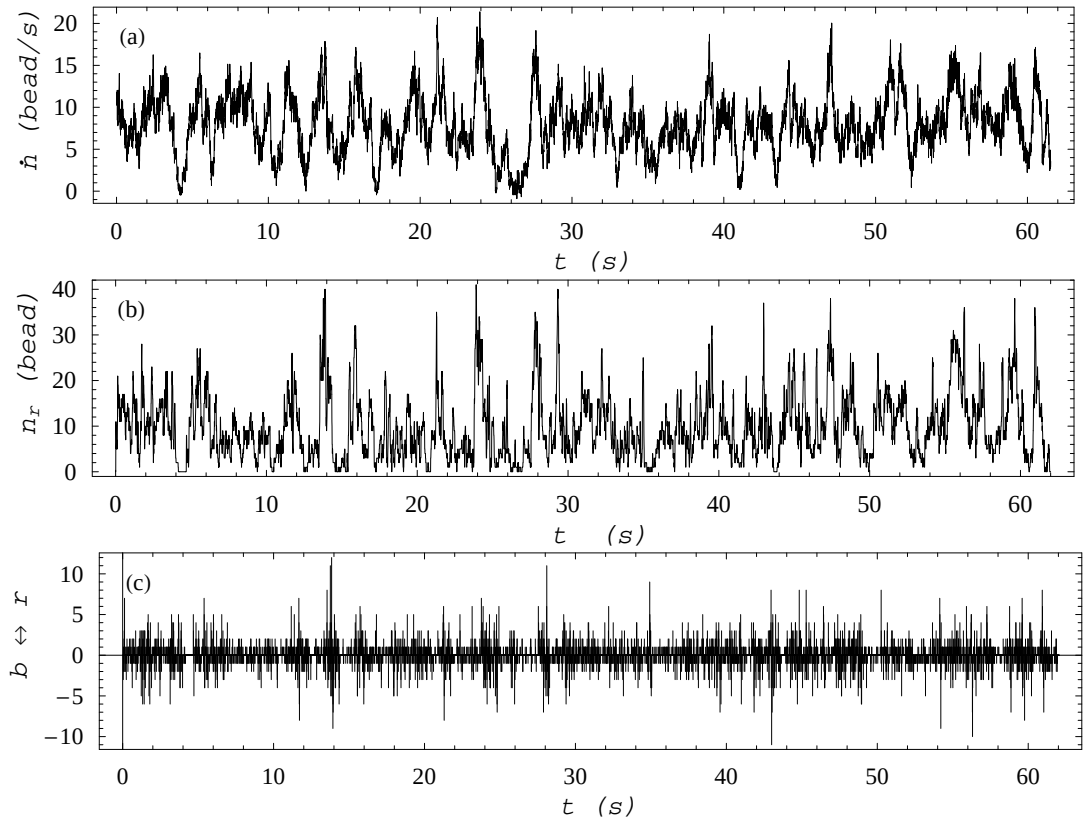

Figure 3. Experiment 10-8: mean solid discharge at the channel inlet $\dot{n}_0 = 8$ beads/s; mean bed slope $\tan\theta = 0.1$. (a) Solid discharge $\dot{n}$ as a function of time. (b) Variation in the number of rolling particles n_r. (c) Exchanges between the bed and the rolling phases: each bar oriented upward indicates the number of beads that passed from the resting state to the rolling regime over a given time interval $\Delta \approx 1/130$ s; downward-oriented bars represent the number of rolling particles coming to a halt.

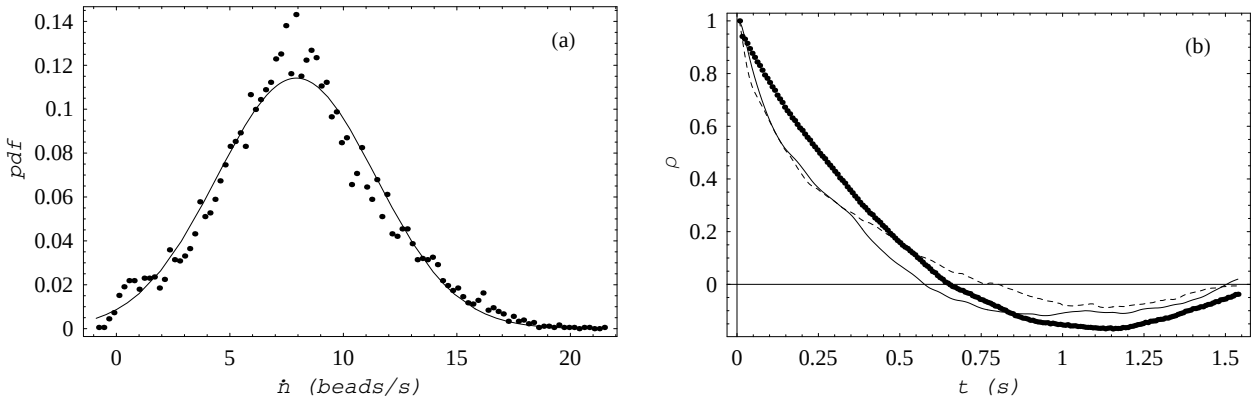

Figure 4. (a) Probability distribution function (pdf) of the solid discharge for experiment E10-8 ($\dot{n}_0 = 8$ beads/s; mean bed slope $\tan\theta = 0.1$): the dots represent the empirical pdf, whereas the solid line is a Gaussian distribution adjusted on the data (mean: 7.93, standard deviation: 3.49). (b) Autocorrelation function for experiment E10-8: the thick dotted line corresponds to the solid discharge $\dot{n}$, the thin solid line to the number of rolling particles n_r, and the dashed line to the number of saltating particles n_s.

ber of moving particles and of their velocities [see Eq. (1)]. Indeed, if the particle velocities are sufficiently agitated (resulting in a random velocity distribution) and the number of moving particles within the observation window varies significantly with time, the law of large numbers supports this expectation.

As expected, the autocorrelation functions ρ of the measured signals $\dot{n}(t)$, $n_r(t)$, and $n_s(t)$ are similar. As shown by Fig. 4(b), the typical behavior is the same: (i) we observe a fairly slow exponential decrease, i.e. for short times, we have $\rho(s) \approx \exp(-t/t_e)$ with t_e a typical time scale; (ii) the typical time scales t_e related to each signal are very close. For experiment E10-8, we found $t_e \approx 230$ ms. The autocorrelation times for other experiments are reported in Table 1.

In an earlier paper (Boehm et al. 2004), the timescale t_e was interpreted as the typical travel time of the moving particles through the observation window. While this interpretation seems reasonable for the solid discharge, there is at first glance no clear reason why this should be so for the number of rolling/saltating particles. One could call on the following explanation for the similarity in the autocorrelation functions: once a particle experiences a transition into another regime, it moves at approximately the same velocity as the mean phase velocity and hence one expects that the autocorrelation time $n_r(t)$ and $n_s(t)$ is somehow related to a travel time. However, since their mean phase velocity was quite different (see Table 1), their autocorrelation times should also be different.

In Sect. 2, we have also shown that for particle entrainment, the waiting-time distribution should follow an exponential distribution of rate $r = N/(\sigma + \tau)$. A particular problem encountered here in evaluating the parameter r is that we could not resolve successive events when they occurred within a very short time interval (less than the acquisition rate of our camera, i.e. for lag times shorter than $2/130 = 0.015$ s); this means that we should censor the lag-time sample to remove the lowest values if we want to properly evaluate the sample distribution. For the sake of simplicity, however, we did not proceed in this way. Figure 5(a) shows the empirical probability distribution function of the lag times Δt for the different classes of events (entrainment or deposition, transition to a rolling or a saltating regime). We have superimposed the exponential distribution, the coefficient of which has been adjusted using the method of moments on the whole sample. As expected, the exponential distribution is a fairly good representation of the lag-time distribution whatever the type of exchange except at low values of Δt, for which the empirical distribution departs significantly from the exponential trend. Adjustment provides the following characteristic times for each transition type for experiment E10-8: $\Delta t_{b\to r} = 33.9$ ms, $\Delta t_{r\to b} = 31.7$ ms, $\Delta t_{r\to s} = 57.4$ ms, and

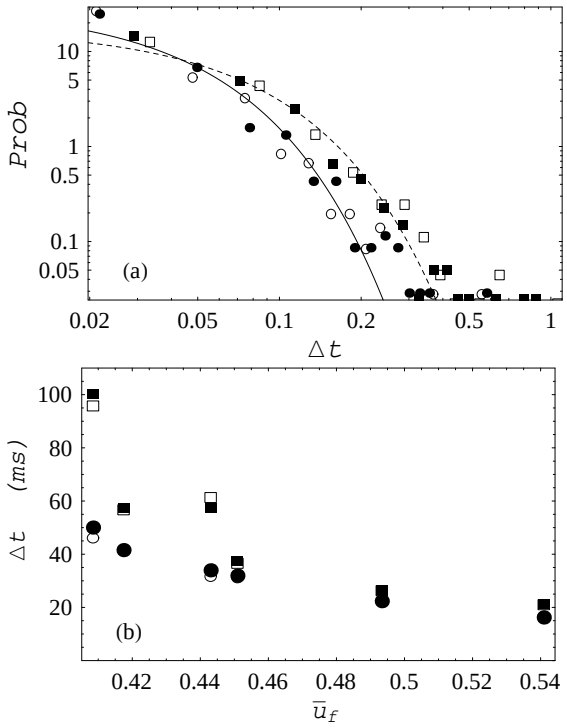

Figure 5. (a) Probability distribution of the time lag Δt between two events (change in state): the filled disks represent the state transition $b \to r$ (entrainment, $\tau_{b\to r}$), while the empty disks represent the state transition $r \to b$ (deposition, $\tau_{r\to b}$); the solid line provides the exponential probability distribution adjusted on the data $b \longleftrightarrow r$ (using the method of moments). The filled boxes represent the state transition $r \to s$, while the empty boxes represent the converse transition $s \to r$; the dashed line is the exponential probability distribution adjusted on the data $r \longleftrightarrow s$. (b) Variation in the lag times $\Delta t_{b\to r}$ (filled disks), $\Delta t_{r\to b}$ (empty disks), $\Delta t_{r\to s}$ (filled boxes), and $\Delta t_{s\to r}$ (empty boxes).

$\Delta t_{s\to r} = 61.3$ ms. For all experiments, the mean lag times are reported as a function of the mean fluid velocity in Fig. 5(b).

Up to this point, the generalized Einstein theory is qualitatively consistent with our laboratory experiments. A discrepancy is, however, noticeable. In Sect. 2, we found that the autocorrelation time t_e was $\tau_* = \sigma\tau/(\tau + \sigma)/N$ and the waiting time was $\Delta t_{b\to r} = r^{-1} = (\sigma + \tau)/N$. From these relations, we deduce that the ratio

$$\frac{\tau_*}{\Delta t_{b\to r}} = \frac{\tau/\sigma}{(\tau/\sigma + 1)^2} < 1,$$

in contradiction with our experimental results, since for instance for E10-8, we have $\tau_*/\Delta t_{b\to r} = 6.9$. The autocorrelation time is much longer than expected. As we shall see in the next subsection, this result is not fortuitous and illustrates the existence of long-range correlations in the physical processes governing sediment transport.

4.2 *Probability distribution of the number of moving particles*

Analyzing the probability distribution of the number of moving particles is richer than examining that of the solid discharge because the latter combines two sources of fluctuations: the number of particles and their velocities, which makes it difficult to properly interpret them. Here, we will focus on the probability distributions of the number of rolling particles n_r (see Fig. 6).

Figure 6 shows how the probability distribution of n_r changes when the fluid velocity is increased. At low fluid velocities, the probability distribution is close to a straight line in a log-linear diagram, revealing a power-like behavior. At higher fluid velocities, the probability distribution takes the shape of an asymmetric bell, with its maximum moving from left to right. At first sight, the prominent impression is that increasing the solid discharge leads to making the probability distribution of n_r more Gaussian.

In the generalized Einstein theory presented in Sect. 2, we inferred that the number of moving particles should be distributed according to a binomial law, with mean ξN and variance $\xi(1-\xi)N$ where N is the density number of particles lying on the bed and $\xi = \tau/(\sigma + \tau)$ is the mean relative time during which a particle is maintained in motion by the stream. A particularity of the binomial law is that its variance must be lower than its mean. For all our experiments, we found that the sample variance exceeded the sample mean. For instance, for experiment E10-8 [see Fig. 6(c)], the mean number of particles is $\bar{n}_r = 10.4$, whereas the variance is $\mathrm{Var}(n_r) = 55.8$. For all probability distributions, the distribution tail is much thicker than expected.

Since thick tails are often associated with collective phenomena (Sornette 2000), it is worthwhile characterizing these distributions more accurately. We found that the negative binomial distribution provides a fairly proper representation of the empirical distribution, as shown in Fig. 6. Small departures are observed in the distribution tail (insufficient number of data) and when $n_r \to 0$. Note that it was not always very easy to distinguish between incipient motion and oscillations of bed particles and consequently our image-processing algorithm failed at times to count the exact number of moving particles. The small deviations between the theoretical and empirical probability distributions may result from this uncertainty on n_r. Except for the behavior close to the boundaries, the whole trend is well represented by the negative binomial distribution. Instead of a discrete distribution, we can use a continuous probability distribution to approximate the empirical distribution of n_r. A natural candidate is the gamma distribution, which can be fairly well adjusted on data, as shown in Fig. 6.

This observation is of fundamental importance since it conflicts with the assumptions underlying the birth-and-death process used in the theoretical derivation. Indeed, if the particles are independent and identical, then one obtains a binomial distribution whatever the model taken for rest/move, provided that the flow is steady and there is bed equilibrium. The only way to obtain a non binomial behavior would be to have (i) unsteady flow conditions or (ii) non identical or dependent particles. Assumption (ii) is the most plausible. Taking a closer look at the resting and moving states showed that on many occasions, particles moved in well-separated groups (Boehm et al. 2004). Collective displacement and entrainment of particles explained why the particles were to some extent dependent and thus why the autocorrelation time was much longer than expected. One might think that aggregate transport was promoted by particle sphericity and equal size. Our observations are, however, well supported by field measurements, which documented similar processes in gravel-bed rivers (Drake, Shreve, Dietrich, & Leopold 1988). The wide range of fluctuations exhibited by laboratory or field measurements (Wilcock 2001; Martin 2003; Barry, Buffington, & King 2004) also confirmed the existence of thick-tailed probability distributions for sediment transport involving irregular particles.

5 CONCLUSION

Our experimental results provided evidence that, although some statistical properties (such as the autocorrelation function of the solid discharge) predicted by Einstein's theory were consistent with our data, the autocorrelation functions of the number of moving particles and their mass distribution functions violated the assumptions underpinning Einstein's theory. Typically, the autocorrelation time was much longer than expected and the mass distribution function had a much thicker tail than predicted using Einstein's arguments. For instance, from the theoretical standpoint, the number of moving particles within any observation window is a random number distributed according to a binomial distribution; in the large-number limit, the theoretical distribution should tend very quickly toward a Gaussian limit. In contrast, our experiments showed that the sample variance outweighed the sample mean and a negative binomial distribution fits the data better. This means that extreme events (i.e., a large number of moving particles) are much more frequent than expected. Furthermore, our experiments showed that the convergence toward the Gaussian limit is slow. At the lowest solid discharges achievable with our system, the probability distribution of the particle number is closer to a power-law distribution. When increasing the solid discharge, the variance/mean ratio decreases and the probability distri-

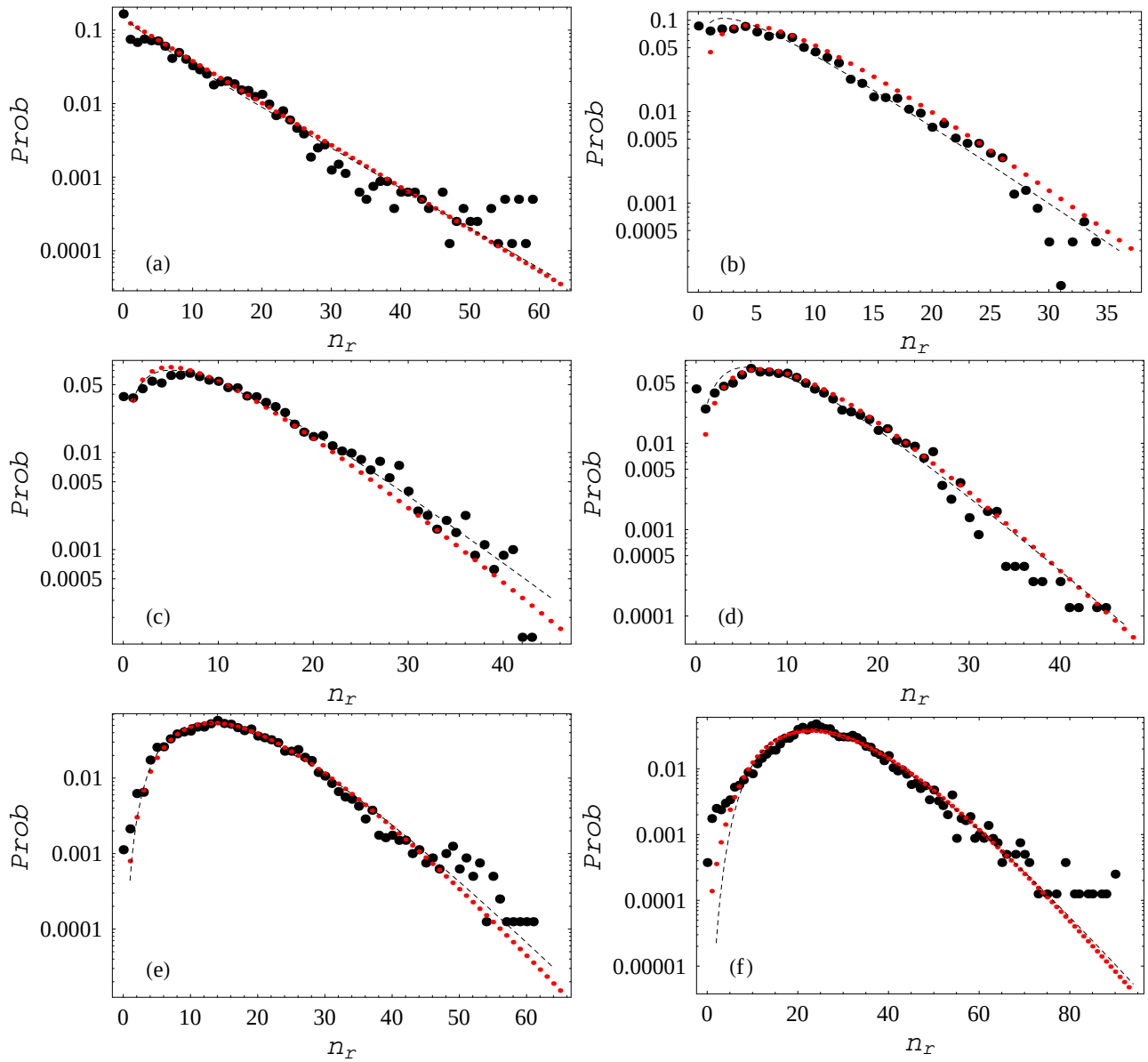

Figure 6. Probability distributions of the number of rolling particles. The dots represent the empirical probability mass functions. The dotted lines represent the negative binomial distribution, while the dashed lines represent the gamma distribution. (a) Experiment E10-6, (b) experiment E10-7, (c) experiment E10-8, (d) experiment E10-9, (e) experiment E10-16, (f) experiment E10-21.

bution becomes increasingly bell-shaped.

The present study has many important implications. First, it provides a plausible explanation about the failure of all mean-field theories on bed-load transport, which ignore any cooperation effects between particles. It thus motivates further research with a clear focus on collective effects in entrainment and displacement of coarse particles as a result of fluid action. Second, this work sheds some light in the critical issues concerning bed-load measurement in rivers (Bunte & Abt 2005). Hydraulicians and geomorphologists use various systems (Helley-Smith sampler, bed-load trap) to measure the solid discharge by capturing sediment over a given time interval. The crux of the issues lies in the proper selection of the sampling time (ranging from a few seconds to several minutes), and this difficulty of selecting a proper timescale is illustrated by the large differences among various measurement systems.

Références

Ancey, C., F. Bigillon, P. Frey, & R. Ducret (2003). Rolling motion of a single bead in a rapid shallow water stream down a steep channel. *Phys. Rev. E 67*, 011303.

Ancey, C., F. Bigillon, P. Frey, R. Ducret, & J. Lanier (2002). Motion of a single bead in a rapid shallow water stream down an inclined steep channel. *Phys. Rev. E 66*, 036306.

Barry, J., J. Buffington, & J. King (2004). A general power equation for predicting bed load transport rates in gravel bed rivers. *Water Resour. Res. 40*, W10401.

Boehm, T. (2005). *Motion and interaction of a set of particles in a supercritical flow*. Ph. D. thesis, Joseph Fourier University.

Boehm, T., C. Ancey, P. Frey, J.-L. Reboud, & C. Duccotet (2004). Fluctuations of the solid discharge of gravity-driven particle flows in a turbulent stream. *Phys. Rev. E 69*, 061307.

Bunte, K. & S. Abt (2005). Effect of sampling time on measured gravel bed load transport rates in a coarse-bedded stream. *Water Resour. Res. 41*, W11405.

Drake, T., R. Shreve, W. Dietrich, & L. Leopold (1988). Bedload transport of fine gravel observed by motion-picture photography. *J. Fluid Mech. 192*, 193–217.

Einstein, H. (1950). The bed-load function for sediment transportation in open channel flows. Technical Report Technical Report No. 1026, United States Department of Agriculture.

Gardiner, C. (1983). *Handbook of Stochastic Methods*. Berlin: Springer Verlag.

Kuhnle, R. A. & J. B. Southard (1988). Bed load transport fluctuations in a gravel bed laboratory channel. *Water Resour. Res. 24*, 247–260.

Lisle, I., C. Rose, W. Hogarth, P. Hairsine, G. Sander, & J. Y. Parlange (1998). Stochastic sediment transport in soil erosion. *J. Hydrol. 204*, 217–230.

Lisle, T. (1989). Sediment transport and resulting deposition in spawning gravels, north coastal California. *Water Resour. Res. 25*, 1303–1319.

Marsh, N., A. Western, & R. Grayson (2004). Comparison of Methods for Predicting Incipient Motion for Sand Beds. *J. Hydraul. Eng. 130*, 616–621.

Martin, Y. (2003). Evaluation of bed load transport formulae using field evidence from the Vedder River, British Columbia. *Geomorphology 53*, 75–95.

Papanicolaou, A., P. Diplas, N. Evaggelopoulos, & S. Fotopoulos (2002). Stochastic incipient motion criterion for spheres under various bed packing conditions. *J. Hydraul. Eng. 128*, 369–390.

Sornette, D. (2000). *Critical Phenomena in Natural Sciences*. New York: Springer.

Wilcock, P. (2001). Toward a practical method for estimating sediment-transport rates in gravel bed-rivers. *Earth Surf. Proc. Landforms 26*, 1395–1408.